Proceedings of the 17th Hypervelocity Impact Symposium
HVIS2024
September 9-13, 2024, Tsukuba, Japan

HVIS2024-095

EVALUATION OF THE AFRP DURABILITY AGAINST DEBRIS CLOUD IMPACTS WITHIN MULTIPLE-LAYERED BUMPER SHIELD STRUCTURES

Ryoya Sano[1], Yukihiro Ishibashi[2], Kai Ito[1], Shoya Iwata[1], Sunao Hasegawa[3], Penelope Wozniakiewicz[4], Luke Alesbrook[4], Gareth Appleby-Thomas[5], Kazuyoshi Arai[2], Hajime Yano[3,1]

[1] Graduate School of Science and Engineering, Hosei University Graduate School, Tokyo, Japan
[2] Faculty of Science and Engineering, Hosei University, Tokyo, Japan
[3] Institute of Space and Astronautical Science, Japan Aerospace Exploration Agency, Kanagawa, Japan
[4] Centre for Astrophysics and Planetary Science, School of Physics and Astronomy, University of Kent, Canterbury, Kent U.K.
[5] Centre for Defence Engineering, Cranfield University, Defence Academy of the United Kingdom, Shrivenham, Swindon, U.K.

ABSTRACT

Spacecraft shields like the Whipple bumper on ESA's Giotto spacecraft, which explored Comet Halley, utilize lightweight composites such as Aramid Fiber Reinforced Plastics (AFRP) for effective protection against hypervelocity impacts by meteoroids and debris. While these materials have been only sporadically used over the past 40 years, due to their higher cost compared to traditional Al alloys and the capacity of larger spacecraft to accommodate heavier bumpers, recent trends to utilize smaller spacecraft such as micro-sats and cube-sats necessitate revisiting AFRP. Our studies demonstrate AFRP's superior durability within multi-layered bumpers through laboratory experiments using three-layer configurations exposed to 2-7 km/s impacts by two-stage light gas guns. AFRP layers show less damage and energy transfer, indicating better performance in dissipating impact energy than Al alloys. AUTODYN hydrocode simulations further validate these findings, showing AFRP's kinetic energy reduction per areal density to be double that of Al alloy, underscoring its higher resilience to extreme velocities and making it a preferable choice for modern spacecraft facing stringent mass constraints.

Keywords: AFRP, Hypervelocity impacts, Hydrocode, Whipple bumper shields

NOMENCLATURE

R_h	Penetration hole radius (mm)
S_h	Area of the penetration hole in the layer (mm^2)
S_d	Damaged area (mm^2)
E	Loss of kinetic energy per unit areal density ($J \cdot cm^2/g$)

1. INTRODUCTION

Many spacecraft are equipped with a defensive structure known as a bumper[1]-[7] to protect the internal components from hypervelocity impact damages by micrometeoroids and orbital debris. Traditionally, metals such as aluminium (Al) alloys and titanium (Ti) alloys have been used for the bumpers of spacecraft. However, recent advances in technology have enabled the moulding of complex shapes, leading to the use of composite materials like Carbon Fibre-Reinforced Plastics (CFRP)[2] and Aramid Fibre-Reinforced Plastics (AFRP)[3],[4]. AFRP and similar composites offer advantages of being lightweight and high strength compared to the metal counterparts, so they have been used for bumper materials in space exploration missions. One example is the Giotto mission, launched in 1985 to observe Comet Halley. The Giotto spacecraft[5],[6] used AFRP for its bumper, which protected it from dust impacts at speeds up to 68.4 km/s as it approached within 600 km of the Comet Halley, allowing it to successfully image the comet's nucleus and to analyse its composition, and the Giotto subsequently explored the Comet Grigg-Skjellerup, too. Additionally, in the ESA's Columbus module on the ISS[7], Kevlar epoxy laminate was used as part of the second wall in the Whipple shield as an intermediate material. This study found that a bumper using Nextel ceramic fabric and Kevlar as intermediate materials has higher defensive capabilities than the Whipple bumper. However, since this bumper uses Nextel ceramic fabric and Kevlar as intermediate materials, it is necessary to evaluate the defensive capabilities of AFRP alone. Despite the proven defensive capabilities of these materials, AFRP has been used intermittently as bumper material for spacecraft over the years. This is likely because earlier missions could afford to allocate

more mass resources for bumpers made of heavier Al alloys, making the more expensive AFRP less attractive. Additionally, there has been little research to advance AFRP bumpers against hypervelocity impacts due to the limited flight opportunities of such spacecraft. In the recent trend of space development, utilization of smaller spacecraft such as micro-sats and cube-sats is rapidly increasing while they face challenges in allocating sufficient mass resources for dedicated, conventional bumper structures. Additionally, in the design of micro-spacecraft, there are not only severe mass constraints but also volume constraints. To install bumpers, their thickness and standoff distance must be minimized while still meeting the required defensive performance. This is a new constraint unique to micro-spacecraft, and this study tackles that challenge. When comparing bumpers, one parameter must be kept constant. The reason for matching the thickness in this study is that, with the miniaturization of spacecraft in future bumper development, the volume ratio occupied by the bumper is expected to increase. Therefore, the thickness of the bumper is considered to affect the total volume, which is an important aspect in spacecraft development. For these reasons, I considered thickness to be an important parameter for bumpers and conducted verification based on the same thickness in this study. Using lightweight and high-strength AFRP, this study contributes to the design of a suitable bumper for such micro-spacecraft[8] in a deep space mission by using lightweight, high-strength AFRP, evaluating its defensive performance, and demonstrating the advantages of AFRP over the metal counterparts as Whipple bumper layers. Additionally, since the thickness of the Al alloy layer and AFRP layer is the same, their areal densities differ. Therefore, the energy loss per areal density is compared.

2. EXPERIMENTS

2.1 EXPERIMENTAL MATERIALS

For our experimental targets, two types of bumpers were employed: the Al bumper made only of Al alloy (Figure 1) and the AFRP bumper which included AFRP (Figure 2).

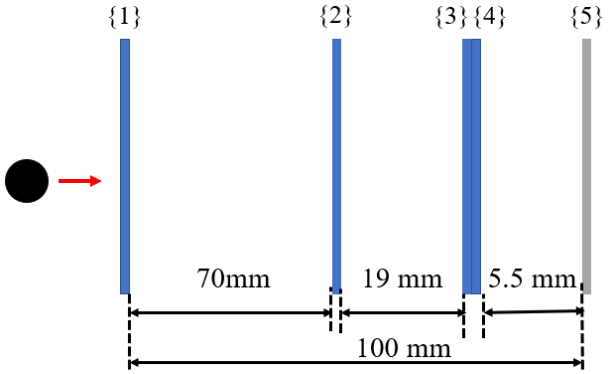

{1}Al t1.0 mm 150× 150 mm	{2}Al t2.0 mm 150× 150 mm	{3}Al t2.0 mm 150× 150 mm	{4}Al t0.5 mm 150× 150 mm	{5}Al t2.0 mm 150× 150 mm

FIGURE 1: THE STRUCTURE OF THE WHIPPLE AL BUMPER (t = THICKNESS)

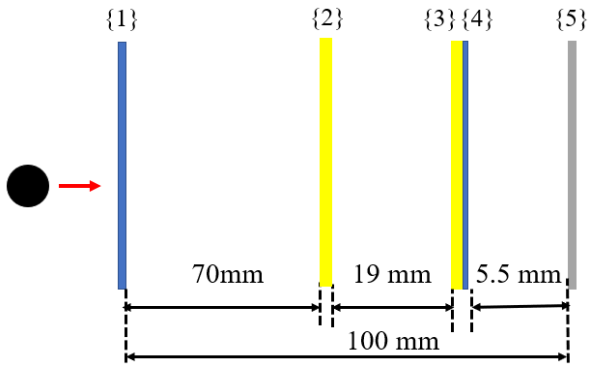

{1}Al t1.0 mm 150× 150 mm	{2}AFRP t2.0 mm 150× 150 mm	{3}AFRP t2.0 mm 150× 150 mm	{4}Al t0.5 mm 150× 150 mm	{5}Al t2.0 mm 150× 150 mm

FIGURE 2: THE STRUCTURE OF THE WHIPPLE AFRP BUMPER (t = THICKNESS)

The Al bumper consists of multiple layers of the first layer {1} through the last layer {5} assumed as a spacecraft interior. All the layers are made of aluminium (Al) alloy (A6061-T6) with respective stand-off distances except the layers {3} and {4} that are bound together. The AFRP bumper consists of the following layers: the first later{1} made of A6061-T6, the second layer {2} made of aramid fibre-reinforced epoxy resin (AFRP), the third{3} layer made of AFRP and the fourth layer {4} made of A6061-T6 laminates are bound together, and the last layer {5} as a spacecraft interior is made of A6061-T6. We employ a laminated configuration of [0/90 ±45 0/90 ±45]s of the AFRP, using Kevlar49 fibres purchased from TMP Corporation. Each layer has dimensions of 150×150 mm, with thicknesses of these layers {1} as 1.0 mm, {2} as 2.0 mm, {3} as 2.0 mm,{4} as 0.5 mm, and {5} as 2.0 mm, respectively. Area densities are 1.49 g/cm^2 for the Al bumper and 0.93 g/cm^2 for the AFRP bumper, respectively. All the hypervelocity impact experiments shot a spherical projectile made of A1050 alloy, with a diameter of approximately 3.2 mm and a mass of 0.045 g.

2.2 EXPERIMENTAL METHODS

The hypervelocity impact experiments were conducted using two-stage light gas guns (TS-LGGs) that were propelled by gunpowder and light gases such as nitrogen, helium, and hydrogen. The impact velocities ranged from 1 km/s to 7 km/s. Details of the shot ID, impact velocity, and experimental locations are listed in Tables 1 and 2.

The TS-LGG at ISAS[9] conducted 11 shots within the velocity range of 2 km/s to 6 km/s. The TS-LGG at Hosei University[10] conducted one shot at 1 km/s. The TS-LGG at the University of Kent[11] conducted three shots within the range of 4 km/s to 5 km/s. The TS-LGG at Cranfield University conducted two shots in the range of 5 km/s to 6.5 km/s.

Additionally, all impact velocities were measured using lasers. Only the shots conducted at ISAS used the HPV-X high-speed camera (Shimadzu, HPV-X) to photograph the

TABLE 1: IMPACT CONDITIONS FOR THE AL BUMPER (ISAS= ISAS/JAXA)

Al_Bumper ID	Impact Velocity [km/s]	Experiment Site
230602-04	2.08	ISAS
230602-05	3.25	ISAS
240327-02	5.92	ISAS
240327-03	4.97	ISAS

TABLE 2: IMPACT CONDITIONS FOR THE AFRP BUMPER (HU= HOSEI UNIVERSITY; ISAS= ISAS/JAXA, UKC= UNIVERSITY OF KENT; CU= CRANFIELD UNIVERSITY)

AFRP_Bumper ID	Impact Velocity [km/s]	Experiment Site
20230706-01-h	1.10	HU
20230601-01	1.55	ISAS
20230601-02	1.79	ISAS
20230602-02	2.15	ISAS
20230601-04	3.25	ISAS
20230601-03	3.32	ISAS
20230602-01	4.10	ISAS
20230705-01	4.22	UKC
20230703-01	4.66	UKC
20230704-01	4.90	UKC
20230706-01	5.02	CU
20230601-05	6.07	ISAS
20230706-02	6.47	CU

hypervelocity impact phenomena with back illumination. After the hypervelocity impact experiments, shapes of each plate of the bumper targets were measured by using a digital microscope to measure 3D morphology (KEYENCE, VR-3200) and ImageJ software.

2.3 NUMERICAL SIMULATIONS

For numerical simulations, impact analysis software (Ansys Autodyn®) was employed, with impact velocities set identical to those in the experiments. Regarding the analytical approach, the A1050 spherical projectile and the central part (20 mm in radius) of the first Al alloy layer {1} were modelled by using the Smoothed Particle Hydrodynamics (SPH) method. Conversely, from 20 mm to 100 mm from the centre of the first layer {1} and the subsequent layers of {2} through {5} were modelled by using the Lagrangian method. The AFRP was treated as quasi-isotropic in the simulations. Material properties of A1050 and A6061-T6[1] were obtained from previous studies, while those of AFRP were determined from tensile tests, bending tests, and thermal conductivity measurements. Additionally, a two-dimensional axisymmetric model was employed. Material models are summarized in Table 3.

TABLE 3: MATERIAL MODELS OF THE PROJECTILE AND THE TARGET ROF THE HYDEOCODE SIMULATIONS

Material	A6061-T6 (Lagrange)	A6061-T6 (SPH)	AFRP (Lagrange)	A1050 (SPH)
Density [g/cm^3]	2.70	2.70	1.30	2.71
EOS	Shock	Shock	Ortho	Shock
Constitutive model	Steinberg Guinan	Steinberg Guinan	Elastic	Piecewise JC
Failure model	Plastic Strain	Plastic Strain	Material Stress/Strain	Johnson Cook
Erosion	Geometric Strain	None	Geometric Strain	None

3. RESULTS AND DISCUSSION

3.1 NUMERICAL SIMULATION VALIDITY

To assess the consistency of the simulations, the penetration and non-penetration areas, as well as the sizes of penetration holes in the first and second layers, were compared with the post-impact targets. When light shone through the back of the target was visible, it was considered as penetration. The area of the penetration holes was calculated using ImageJ for regions where light penetrated. For simulations, the area of the penetration holes was assumed to be circular with a radius R_h (Figure 3).

Table 4 presents by which bumper layer impact damages are stopped for both experiments and simulations. The AFRP bumper stopped the projectile at the 4th layer at 2.15 km/s and at the 3rd layer at 6.072 km/s, whereas the Al bumper stopped the projectile at the 3rd layer at 2.08 km/s and at the 2nd layer at 5.92 km/s. From Table 4, the consistency between the experimental and simulated results was confirmed except for the Al bumper results at 4.97 km/s.

Figures 4 and 5 show the relationship between impact velocity and penetration hole area in the first and second layers for both experiments and simulations.

In Figure 4, it is apparent that there is good consistency between the experimental and numerical results for Al and AFRP bumpers. However, the maximum error of about 55% occurred only at velocities of 2.15 km/s and 6.07 km/s, suggesting that they could be outliers.

In Figure 5, there is also good consistency penetration hole areas in the second layer for both Al and AFRP bumpers. The maximum error of 43% was observed at 4.90 km/s. At 6.07 km/s and 6.47 km/s, no visible light by back illumination was observed through the second layer of the AFRP bumpers because fragmented fibres were tangled and covered the penetrated holes, which were marked by green dots in Figure 5, but the third layer still exhibited impact-damaged areas. Also, be warned that there appear to be fewer plots for the Al bumper simulation results than the Al bumper experimental results in Figures 4 and 5 because some simulation plots are overlapped by the experimental plots.

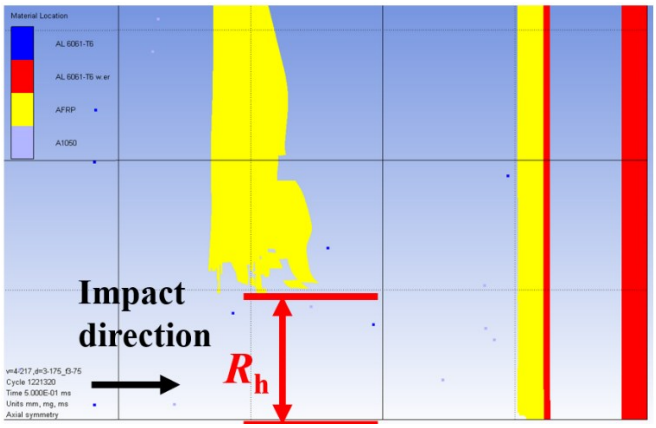

FIGURE 3: EXAMPLE OF NUMERICAL SIMULATION RESULTS FOR THE LAYERS {2}-{5} OF THE AFRP BUMPER

TABLE 4: AFRP IMPACT RESULTS OF IMPACT VELOCITY AND THE LAYER WHERE DAMAGE STOPPED IN EXPERIMENTS AND SIMULATIONS

Velocity [km/s]		Experiment	Simulation
AFRP Bumper	1.10	{4}	{4}
	1.55	{4}	{4}
	1.79	{4}	{4}
	2.15	{4}	{4}
	3.25	{3}	{3}
	3.32	{3}	{3}
	4.10	{3}	{3}
	4.22	{3}	{3}
	4.66	{3}	{3}
	4.90	{3}	{3}
	5.02	{3}	{3}
	6.07	{3}	{3}
	6.47	{3}	{3}
Al Bumper	2.08	{3}	{3}
	3.25	{3}	{3}
	4.97	{3}	{2}
	5.92	{2}	{2}

Taking these cautions into consideration, the general trend of experimental results on the first and second layers is adequately reproduced by the numerical simulations.

For example, the penetration hole area increases as the impact velocity increases in Figure 4 while the maximum value of the penetration hole area appears around 4 km/s in Figure 5.

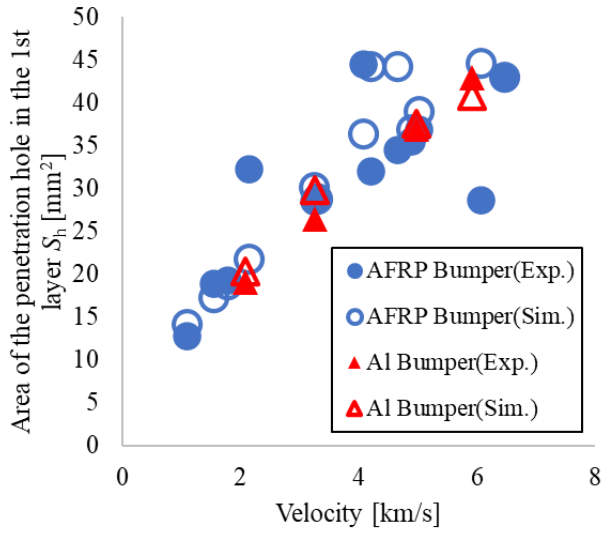

FIGURE 4: THE RELATIONSHIP BETWEEN THE AREA OF THE PENETRATION HOLE IN THE FIRST LAYER AND THE VELOCITY FOR BOTH AL AND AFRP BUMPERS

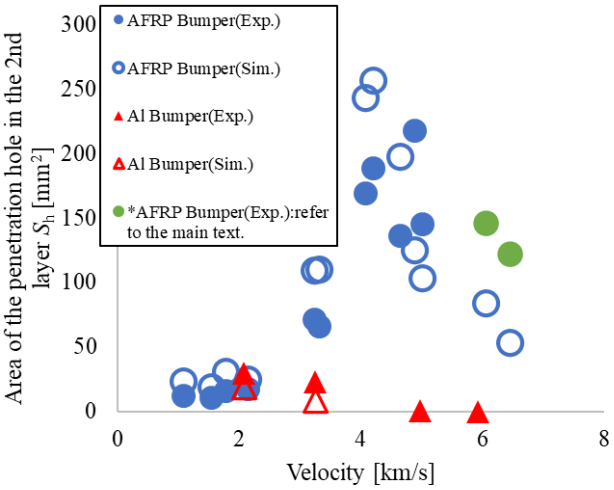

FIGURE 5: THE RELATIONSHIP BETWEEN THE AREA OF THE PENETRATION HOLE IN THE SECOND LAYER AND THE VELOCITY FOR BOTH AL AND AFRP BUMPERS

3.2 EXPERIMENTAL RESULTS

Figure 6 shows examples of damaged areas on the third layer of both Al and AFRP bumpers by TS-LGG impact experiments at approximately 2-3 km/s. A spherical indentation remains around 2 km/s while the damaged areas are more dispersed and scattered around 3 km/s.

Figure 7 shows the relationship between the impact velocity and the damaged area per unit areal density, calculated by dividing the damaged area formed on the third layer by the areal density of the first and second layers for each bumper. The total areal density of the first and second layers is 0.81 g/cm² for the Al bumper and 0.53 g/cm² for the AFRP bumper, respectively. Both the Al and AFRP bumpers increase damaged

areas by around 2 km/s, with a trend change of around 3 km/s where the damaged area decreases.

As witnessed by high-speed camera imagery, even after impacting the first layer below 2 km/s, the projectile maintained its spherical shape, penetrated the second layer, and stopped at the third layer with smaller damaged areas. The projectile shattered upon impacting the first layer above 2 km/s and formed a debris cloud that penetrated the second layer and resulted in larger damaged areas on the third layer. The damaged area got smaller for the impact of the first layer beyond 3 km/s because further fragmentation of the projectile reduced the kinetic energy of the debris cloud, compared to the impacts below 3 km/s.

In Figure 7, it was also found that the damaged areas on the third layer are larger for the AFRP bumper than the Al bumper at all the velocity ranges.

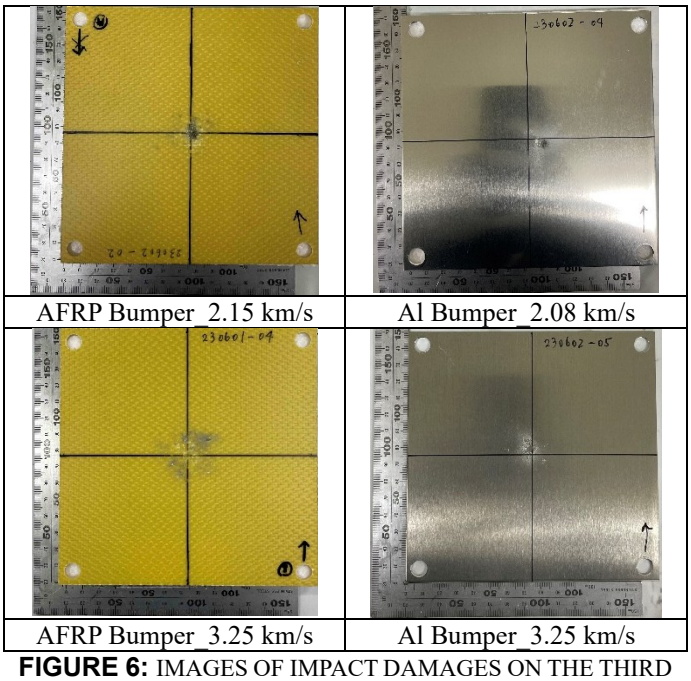

FIGURE 6: IMAGES OF IMPACT DAMAGES ON THE THIRD LAYER OF EACH BUMPER AROUND 2-3 KM/S

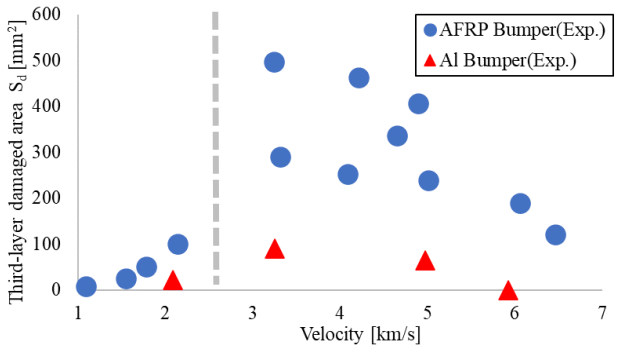

FIGURE 7: DAMAGED AREA ON THE THIRD LAYER FOR BOTH AL AND AFRP BUMPERS

The AFRP bumper produced shattered fibres that caused the fibrous fragment cloud to spread widely after penetrating the second layer. Thus, the breakdown of the AFRP layer into fibrous fragments results in smaller fragment masses, which effectively attenuate the impact energy as each fragment carries less kinetic energy.

3.3 SIMULATION RESULTS

Figure 8 displays the kinetic energy loss per unit of areal density for both the AFRP and Al bumpers. We calculated the loss of kinetic energy when the debris cloud formed by the first layer penetration impacted the second layer using numerical simulations for both the Al and AFRP bumpers. While kinetic energy dissipates more for both bumper types as a function of impact velocities to the first layer, the energy dissipation for the AFRP bumper is about twice as efficient as that of the Al bumper at all the velocity ranges tested (i.e., 2.10-2.17 times at 2-6 km/s). The approximation curves and plots for both Al and AFRP bumpers are sufficiently accurate with a coefficient of determination R^2 of 0.99. This effect is attributed to the high tensile strength and low stiffness of AFRP, which allow it to absorb impact energy and disperse it by stretching the fibres. This significant reduction in kinetic energy means that AFRP can achieve approximately 50 % mass reduction compared to the Al alloy while maintaining the same protection against hypervelocity impacts. While AFRP may provide better protection than Al, further experimental and simulation data are needed to determine the mass benefits of AFRP compared to Al. This includes comparisons of bumpers with the same areal density and the use of AFRP as intermediate and rear wall materials.

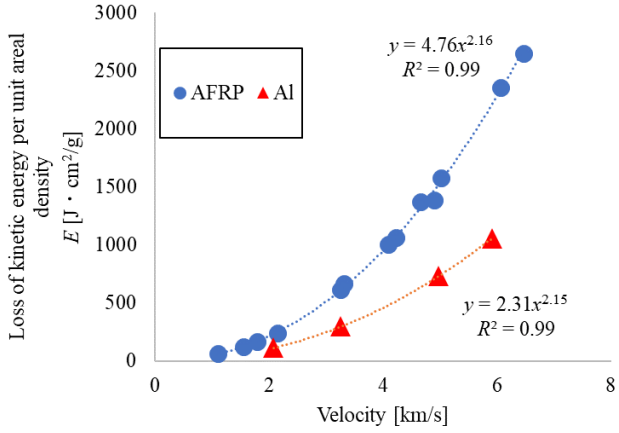

FIGURE 8: THE RELATIONSHIP BETWEEN IMPACT VELOCITY AND ENERGY LOSS PER UNIT AREAL DENSITY FOR BOTH AL AND AFRP BUMPERS

4. CONCLUSION

It was found that AFRP plates can absorb approximately twice as much impact energy per unit areal density as Al alloy plates. Thus, AFRP provides an effective option for lightweight spacecraft bumpers, making it attractive for future spacecraft with smaller mass resources than conventional spacecraft.

ACKNOWLEDGEMENTS

The LGG experiments in this study were conducted with the support of impact experiment facilities at ISAS/JAXA, the University of Kent, and Cranfield University. Additionally, this work used computational resources from the Laboratory provided by the Research Centre for Computing and Multimedia Studies, Hosei University. The authors appreciate all the parties involved for their contributions.

REFERENCES

[1] Arai, K., Takahashi, H., Urasawa, and Hasegawa. S. "Ballistic Limit Velocity of Space Debris Shield used Liquid Layer." *Aerospace Technology,* Vol. 11 (2012): pp. 117-122. (in Japanese)

[2] Nagao, Y., Kibe, S., Daigo, K., and Hara, A. "Damage regions and residual strength in carbon fibre composites due to hypervelocity impacts." *The Materials Science Society of Japan,* Vol. 35 No.1 (2009): pp. 15-26.

[3] Wan, H., Bai, S., Li, S., Mo, J., Zaho, S., and Song, Z. "Shielding performances of the designed hybrid laminates impacted by hypervelocity flyer." *Materials and Design*, Vol. 52. (2013): pp.422-428.

[4] Bao, J., Wang, Y., An, R., Cheng, H., and Wang, F." Investigation of the mechanical and ballistic properties of hybrid carbon/aramid woven laminates." *Defence Technology,* Vol.18 No.10 (2022): pp.1822-1833.

[5] McDonnell, J.A.M. "HVI Phenomena: Applications to space missions." *International Journal of Impact Engineering,* Vol. 23. No.1 (1999): pp. 597-619.

[6] Alexander, W.M. and McDonnell, J.A.M. "Hypervelocity impact on the Giotto Halley mission dust shield: momentum exchange and measurement." *Advances in Space Research,* Vol. 2 No.12 (1982): pp. 185-187.

[7] Christiansen, E.L. "Meteoroid/debris shielding" TP-2003-210788. NASA Johnson Space Centre, Houston, Texas. 2003.

[8] Machuca, P., Ozaki, N., Sanchez, J.P., and Felicetti, L. "Dust impact and attitude analysis for JAXA's probe on the Comet Interceptor mission" *Advances in Space Research,* Vol. 70. (2022): pp. 1189-1208.

[9] Kawai, N., Tsurui, K., Hasegawa, S., and Sato, E. "Single microparticle launching method using two-stage light-gas gun for simulating hypervelocity impacts of micrometeoroids and space debris" *Review of Scientific Instruments* Vol. 81 No. 11 (2010)

[10] Fujiwara, A., Kadono, T., and Nakamura, A. "Cratering Experiments into Curved Surfaces and Their Implication for Craters on Small Satellites" *Icarus* Vol. 105 No.2 (1993): pp. 345-350

[11] Ruth, H., Cole, M.J., Price, M.C., and Burchell, M.J. "The Hypervelocity Impact Facility at the University of Kent: Recent Upgrades and Specialized Capabilities." *Procedia Engineering,* Vol. 204 (2017): pp. 208-214.